

NANO EXPRESS

Open Access

Controllable synthesis porous Ag_2CO_3 nanorods for efficient photocatalysis

Shenghui Guo^{1,2,3,4}, Jianxing Bao^{1,2,3,4}, Tu Hu^{1,2,3,4}, Libo Zhang^{1,2,3,4}, Li Yang^{1,2,3,4*}, Jinhui Peng^{1,2,3,4} and Caiyi Jiang^{1,2,3,4}

Abstract

The novel porous Ag_2CO_3 nanorods were facilely synthesized via a one-pot aqueous solution reaction at room temperature. The crystalline phase and size distribution of the nanorods were determined by X-ray diffraction (XRD) and scanning electron microscopy (SEM), respectively. In addition, the porous feature of nanorods was confirmed by transmission electron microscopy (TEM) and nitrogen adsorption-desorption. The morphology and size of the Ag_2CO_3 crystal can be regulated via the choice of dispersing agents and adding approaches of reactants. Photocatalytic results show that the porous Ag_2CO_3 nanorods exhibit excellent photodegradation of rhodamine B (RhB) under visible-light irradiation, particularly the photoactivity performance and stability can be further improved in the presence of sodium bicarbonate (NaHCO_3). It is indicated that NaHCO_3 can prevent effectively the photocorrosion and promote the probability of electron-hole separation.

Keywords: Crystal growth; Porous nanorods; Silver carbonate; Photocatalysis

Background

Semiconductor photocatalysts have attracted intense attention expecting to apply in the fields of pollution removal and fuel production by utilizing abundant sunlight [1-3]. Over the past years, TiO_2 as the most universal used photocatalyst has been widely studied owing to its high photocatalytic activity, stability, non-toxicity, and low cost [4-7]. However, TiO_2 is a wide bandgap (approximately 3.2 eV) semiconductor and difficult to be activated in visible-light region, only can be utilized under UV light which is a small fraction (about 4%) of the entire solar spectrum. In addition, TiO_2 quantum yield of photoactivated processes is frequently lower due to its high recombination of photogenerated electron-hole pairs. Such clear drawback is the main motivation for searching a new, active under visible-light-driven and more efficient photocatalysts [8-10].

Recently, it has been found that silver-containing complex oxide semiconductors show great promise for improving photocatalytic performance owing to their tops

of valence band can form a new higher-energy valence band consisting of the hybrid orbital of Ag 4d and O 2p, which make the bandgap narrower [11,12]. As a result, a series of visible-light-responsive novel silver-containing complex oxide semiconductor photocatalysts have been developed, such as AgNbO_3 [13,14], AgSbO_3 [12,15], Ag_2CrO_4 [16,17], Ag_2SO_3 [18], Ag_3AsO_4 [19], AgMO_2 ($M = \text{Al, Ga, In}$) [20], and AgIO_4 [21], and their active visible-light-driven photocatalysts for the degradation of organic pollutants have also been explored. More recently, it was reported that Ag_2CO_3 showed high-efficiency visible-light activity and exhibited universal degradation ability for typically several organic dyes [22-24]. However, the photocorrosion behavior of Ag_2CO_3 exposed to the light irradiation cannot be ignored. Hence, the addition of light stabilizer in reaction solution is critical to Ag_2CO_3 photocatalyst for its practical application. Dai et al. [23] prepared Ag_2CO_3 short rods by a simple precipitation reaction, and it showed that high visible-light photocatalytic activity for the photodegradation of rhodamine B (RhB). The authors stated that the silver nitrate (AgNO_3) is beneficial to the stability during the photocatalytic degradation reaction process because it can act as an electron acceptor to avoid photocorrosion of Ag_2CO_3 photocatalyst. Moreover, it has been reported that the photocatalytic efficiency can be further improved by rational design to achieve

* Correspondence: yanglikmust@163.com

¹State Key Laboratory of Complex Nonferrous Metal Resources Clean Utilization, Kunming University of Science and Technology, Kunming 650093, China

²National Local Joint Laboratory of Engineering Application of Microwave Energy and Equipment Technology, Kunming 650093, China

Full list of author information is available at the end of the article

porous structures, in that, the porous structures avail the adsorption of reactant molecules and provide multiple accessible passages which reduce the reactant diffusion distance due to their large specific surface area (SSA). Significantly, porous structure can produce more isolated and separated active sites after photoirradiation and provide special channels for charge transport, which results in high efficiency of charge separation and transport in under photoirradiation [25-27].

As far as we know, the synthesis of porous silver-containing complex oxide photocatalysts by one-pot aqueous solution reaction at room temperature has rarely reported. Herein, in the present work, we prepared a novel porous Ag_2CO_3 nanorod photocatalyst by one-pot aqueous solution reaction using PVP-K90 dispersing agent at room temperature. The as-prepared samples showed efficient photocatalytic activity for the degradation RhB aqueous solution by utilizing sodium bicarbonate (NaHCO_3) as a light stabilizer under visible-light irradiations. Furthermore, the growth behavior of Ag_2CO_3 and photocatalysis enhanced mechanism of NaHCO_3 were also discussed.

Methods

Materials

All the chemicals were analytic grade purity and were used without further purification. AgNO_3 , NaHCO_3 , polyvinylpyrrolidone (PVP-K30, PVP-K90) and RhB were purchased from Shanghai Chemical Regent Factory of China (Shanghai, China).

Synthesis of porous Ag_2CO_3 nanorods

The porous Ag_2CO_3 nanorods were synthesized by a typically simple aqueous solution reaction at room temperature. In a typical synthesis, AgNO_3 (0.025 M) and PVP-K90 (0.45 M) were dissolved in 40 mL deionized water to form a clear solution by magnetic stirring, then, 40 mL aqueous solution of NaHCO_3 (0.05 M) was dropwise added to the obtained solution. The reaction was carried out at room temperature for 2 h under magnetic stirring, and the precipitate was collected by centrifugation, washed three times with deionized water and absolute ethyl alcohol, and dried at 50°C for 12 h. Furthermore, the synthesis of Ag_2CO_3 thin nanorods was similar to the above description except that PVP-K90 was replaced by PVP-K30. The cube-like Ag_2CO_3 was achieved by one-time injection of the NaHCO_3 solution using PVP-K90 as the dispersing agent. N-doped TiO_2 , which is good photocatalytic activity under visible-light irradiation, was obtained as a reference to compare with our sample according to the reported literature [28].

Characterization

Scanning electron microscopy (SEM) images were taken using a field-emission scanning electron microscope

(JSM-6701 F, JEOL Ltd., Akishima-shi, Japan) and equipped with an energy-dispersive (ED) detector with this field-emission scanning electron microscope (FE-SEM) operated at 15 kV. Energy-dispersive X-Ray (EDX) analysis was also performed on the JSM-6701 F instrument during SEM. Transmission electron microscopy (TEM) images were obtained on a JEM-2100 electron microscope (JEOL Ltd., Akishima-shi, Japan) at an accelerating voltage of 200 kV. X-ray diffraction (XRD) data for the finely ground samples were collected at 298 K using a Bruker D8 X-ray diffractometer (Bruker AXS, Inc., Madison, WI, USA) with $\text{Cu-K}\alpha$ radiation source ($\lambda = 1.5406 \text{ \AA}$). It was operated at 40 kV in the 2θ range of 10° to 80° in the continuous scan mode with the step size of 0.01° . The changes in the oxidation state of Ag were recorded through an AXIS-ULTRA DLD-600 W photoelectron spectrometer (Shimadzu Corporation, Kyoto, Japan) (XPS) with Al K1 radiation. Nitrogen adsorption-desorption isotherms were collected on an Autosorb-iQ sorption analyzer (Quantachrome Instruments, Boynton Beach, FL, USA) and analyzed followed by the Brunauer-Emmett-Teller (BET) equation. The pore size distribution plots were obtained by using the Barret-Joyner-Halenda (BJH) model.

Photocatalytic performance measurements

The photocatalytic performance of the as-prepared samples was evaluated by measuring the degradation of RhB. In all catalytic activity of experiments, the samples (0.05 g) were put into a solution of RhB dyes (50 mL, 10 mg/L), which was then irradiated with a 300-W Xe arc lamp to provide visible light with $\lambda \geq 420 \text{ nm}$ by an ultraviolet cutoff filter. Before the suspensions were irradiated, they were magnetically stirred for 30 min in the dark to complete the adsorption-desorption equilibrium between dyes and photocatalysts. The degradation of RhB was monitored by UV-vis spectrophotometer (UV-2550, Shimadzu Corporation, Kyoto, Japan) every 5 min. Before the spectroscopy measurement, these photocatalysts were removed from the photocatalytic reaction systems by centrifugation. The relative concentrations (C/C_0) of the RhB solutions were determined by the absorbance (A/A_0) at 553 nm.

Results and discussion

The porous Ag_2CO_3 nanorods were successfully synthesized by the precipitation reaction between AgNO_3 of aqueous solution in the presence of PVP-K90 and NaHCO_3 at room temperature. Figure 1A,B shows typical morphology of samples with different magnifications. From Figure 1A, it can be clearly seen that the products are uniformly dispersed and present nanorod morphology with length of about 3 μm and diameter of 300 nm. Moreover, the high-magnification SEM image in Figure 1B indicates that the surface of the Ag_2CO_3 nanorods displayed

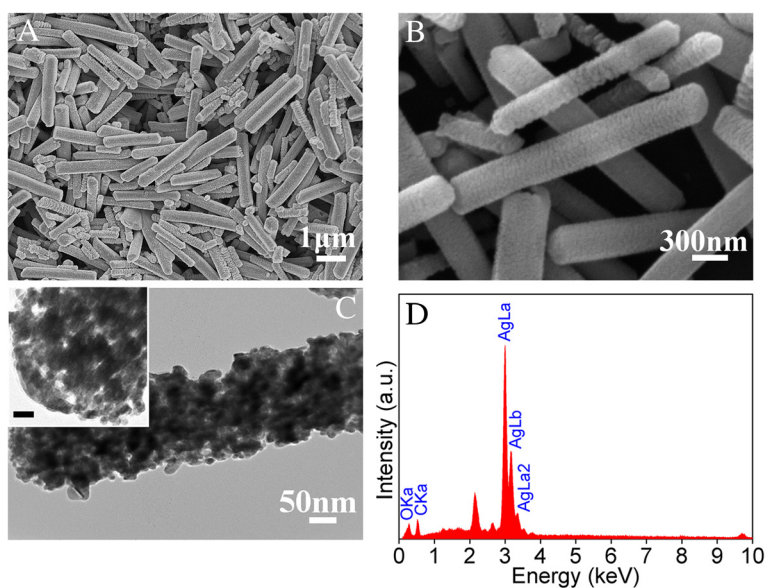


Figure 1 SEM, TEM images, and EDS pattern. **(A, B)** Low- and high-magnified SEM images. **(C)** TEM images (inset scale bar = 20 nm). **(D)** EDS pattern of as-prepared Ag_2CO_3 samples.

certain roughness, which implies that the nanorods are of porous feature. To get more information about the morphology and interior feature of the Ag_2CO_3 nanorods, the TEM technique was used to investigate of the Ag_2CO_3 nanorods. As shown in Figure 1C, a typical TEM image of the as-prepared products and a mass of holes are distributed on Ag_2CO_3 nanorods and every nanorod is assembled by many Ag_2CO_3 nanocrystal grains. In addition, energy-dispersive X-ray spectroscopy (EDS) spectrum (Figure 1D) indicates that the Ag_2CO_3 samples only contain C, O, and Ag elements except for the elements of Au from the supports, proving that the obtained products are composed of pure Ag_2CO_3 .

To further study the surface area and porous feature of Ag_2CO_3 samples, N_2 adsorption-desorption isotherms were also measured. As shown in Figure 2, the isotherm of samples can be identified as the type IV and H3-type hysteresis loop in the IUPAC classification [29], indicating that the samples are of mesoporous feature. According to the fitting analysis with the BET equation, the surface area is $8.16 \text{ m}^2/\text{g}$, which is much greater than Ag_2CO_3 short rods ($0.91 \text{ m}^2/\text{g}$) as reported in other literature [24]. Furthermore, as shown in the inset of Figure 2, the main pore size distribution is about 3.6 nm, which is good consistent with TEM observation. The formation of mesoporous is attributable to the loose aggregation of the originated nanoparticles [30,31].

The X-ray diffraction (XRD) was further used to characterize as-prepared Ag_2CO_3 samples. As shown in Figure 3, the Ag_2CO_3 nanorods prepared with PVP-K90 as the dispersing agent intense diffraction peaks at 2θ values of 17.6° , 19.3° , 32.8° , 33.8° , 39.2° , 48.5° , 52.7° , 60.4° ,

and 67.7° correspond to the planes of (101), (110), (211), (300), (220), (222), (410), (330), and (304). All diffraction peaks can be indexed to the typical trigonal structure Ag_2CO_3 crystal (JCPDS No. 31-1236) and no other diffraction peaks are detected, indicating that the obtained products are pure phase Ag_2CO_3 and further confirm by means of EDS characterization (Figure 1D).

Furthermore, a potential reaction approach explaining the above growth process, as the schematic illustration, is shown in Figure 4A. The synthesis procedure mechanism can be understood as follows. Firstly, Ag^+ ions and PVP molecules could form Ag^+ -PVP complex ions when the dissolution of PVP and AgNO_3 in the deionized water under magnetic stirred with an appropriate frequency [32].

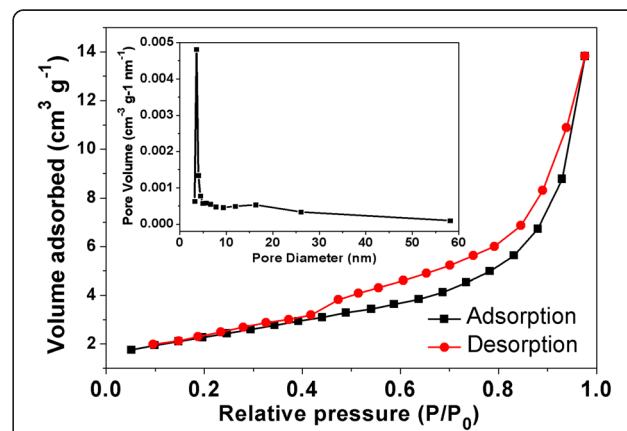
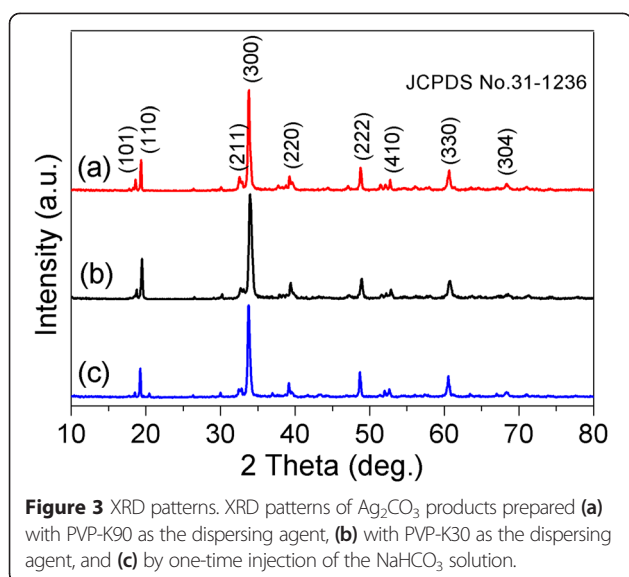


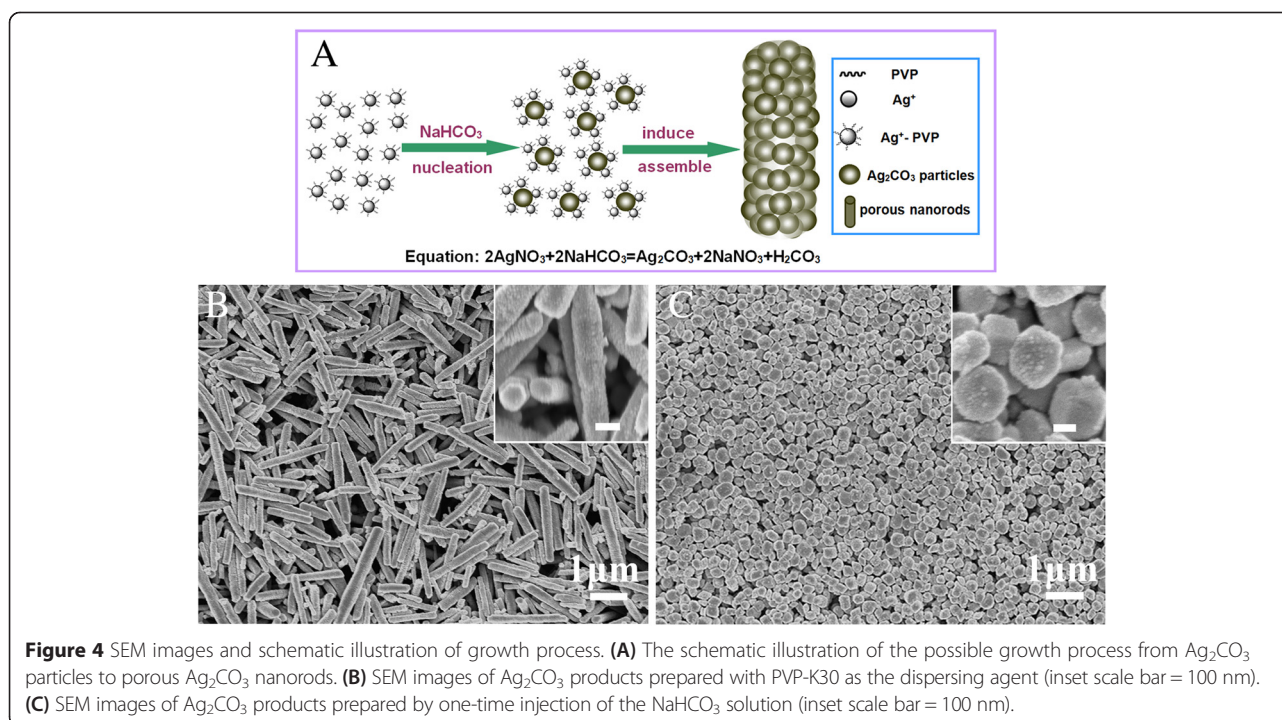
Figure 2 Nitrogen adsorption-desorption isotherm. Nitrogen adsorption-desorption isotherms of as-prepared porous Ag_2CO_3 nanorods. Inset: the pore size distribution of the crystals.

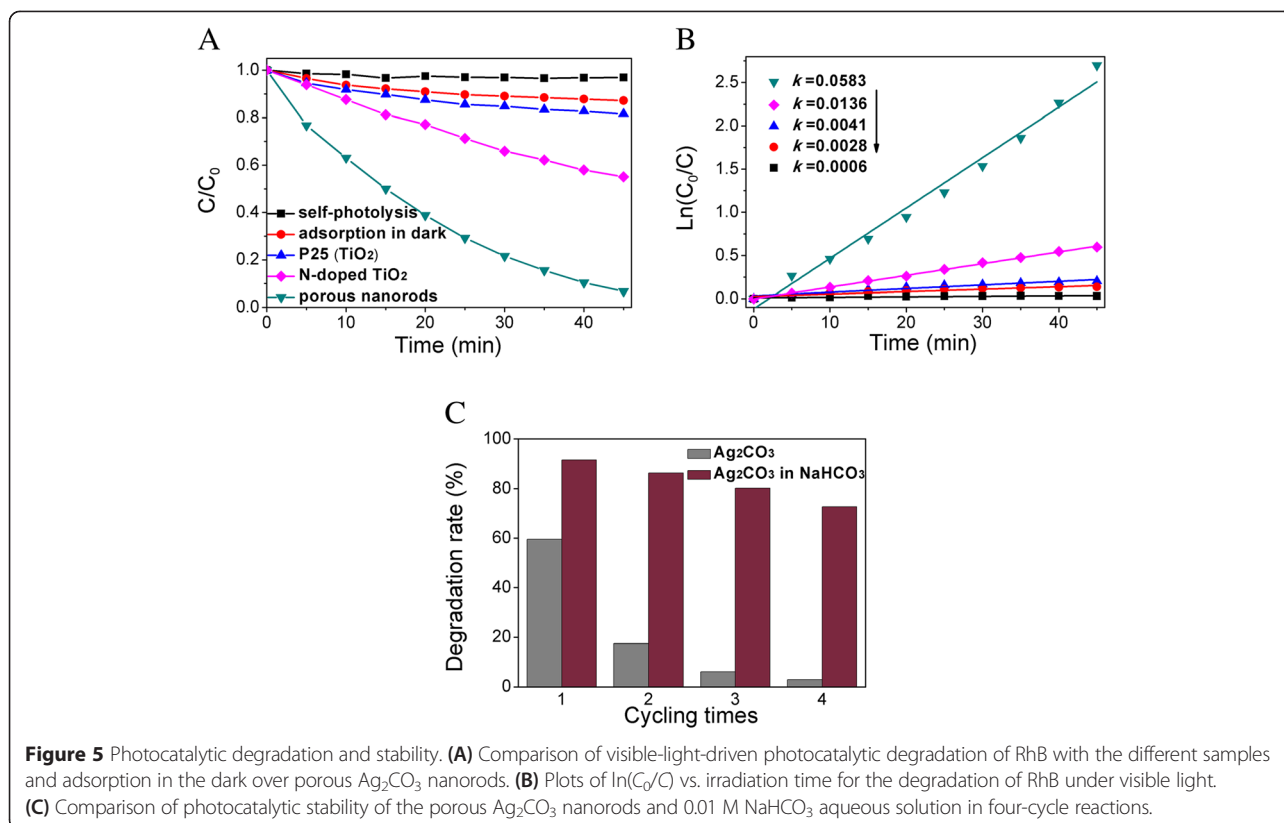


The formed Ag^+ -PVP complex nucleate with CO_3^{2-} and quickly grew into uniform small Ag_2CO_3 nanocrystal grains with preferential (300) crystal plane, while the grains are difficult to continue growing because of isolation effect results from the surface cladding by PVP. As the reaction process continues, a large number of tiny grains assemble into nanorods via the induced effect of PVP long-chain molecules [33-35]. Due to the isolation effect of PVP dispersing agents and the intercrystallite void of aggregation procedure, there exists pore space among adjacent Ag_2CO_3 grains and it eventually evolves into the porous nanorod

structure. In addition, we investigated the relationship between geometrical morphology of nanorods and the category of dispersing agents. When K30 was used in the reaction system, the Ag_2CO_3 nanorods obviously transform thinner and shorter (Figure 4B) by comparing with the as-prepared Ag_2CO_3 nanorods with K90. It is ascribed that K30 has smaller molecular weight, shorter molecular chain length, and lower viscosity than K90, thus result in a weaker adsorption and induced effect in the process of assembly. Furthermore, the adding method of NaHCO_3 solution is also an important influence factor for the evolution of Ag_2CO_3 morphology. When accelerating the drop rate of NaHCO_3 solution, the morphology of as-prepared Ag_2CO_3 becomes small cube-like with the size of about 200 nm; however, it still have a few short nanorods (Figure 4C). These changes may be related to exorbitant instantaneous concentration of CO_3^{2-} , which leads to Ag_2CO_3 explosive nucleation and rapid growth in short time. Owing to the isolation effect of PVP, the formed crystal particles spontaneously start ordered assembly as the aforementioned. However, the assembly process will terminate once CO_3^{2-} specie completely consumed in the reaction system, and it means that the crystal particles will not continue to assemble following by two end face direction. Naturally, the morphology of Ag_2CO_3 samples exhibit cubic trait rather than nanorod. As a consequence, we believe that the geometrical morphology of Ag_2CO_3 can be regulated expediently by the design of experimental conditions.

The photocatalytic activity of as-prepared porous Ag_2CO_3 nanorods was evaluated by the degradation of

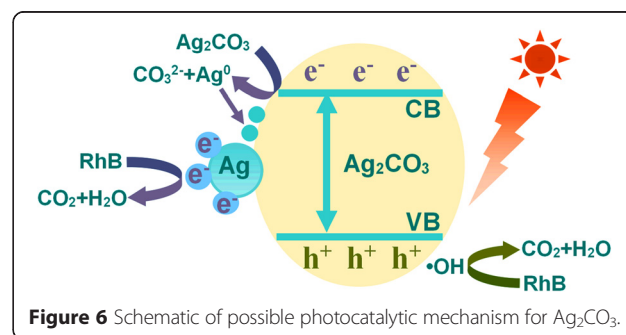




typical water pollutants, RhB under visible-light irradiation at room temperature. As is shown in Figure 5A, the self-degradation effect of RhB could be ignored. What is more, by comparing to the photocatalytic performance of as-prepared Ag_2CO_3 samples and N-doped TiO_2 under visible-light irradiation, it indicates that the photocatalytic activity of porous Ag_2CO_3 nanorods is superior to N-doped TiO_2 . The degradation rate of porous Ag_2CO_3 nanorods can reach 94% within 45 min to RhB, while the latter only 45% in the same experimental conditions. Meanwhile, the kinetic process of the photocatalytic degradation reaction was investigated, as shown in Figure 5B. It is observed that the photocatalytic degradation reaction process follows pseudo-first-order kinetic feature with rate constant k of 0.0583 min^{-1} for porous Ag_2CO_3 nanorods, which show much higher degradation rate than the N-doped TiO_2 and P25 (0.0136 min^{-1} and 0.0033 min^{-1} , respectively). It benefits from more surface active sites and larger specific surface area for the porous structure and ultimately leads to the increase of contact area between materials and target pollution [25,26].

The stability of the Ag_2CO_3 is another vital consideration except for the photocatalytic activity. It is well known that most silver compounds are light sensitive and appear metallic silver when exposed to light, including Ag_2CO_3 photocatalyst [22,23,36]. To evaluate the stability of the photocatalyst, the recycle experiments of

RhB degradation over porous Ag_2CO_3 nanorods were conducted, and the result is shown in Figure 5C. It was found that after four-time cycles, the degradation efficiency of Ag_2CO_3 would decrease from 60% to 3%, indicating that Ag_2CO_3 was unstable in the absence of imperative stabilizers under visible-light irradiation. Two possible mechanisms are proposed to explain the photocatalytic activity decreased and instability (Figure 6). Ag_2CO_3 belongs to indirect bandgap semiconductor with a bandgap about 2.30 eV [23,24]; hence, the electrons can be effectively activated from the valence band (VB) to conduction band (CB) under visible light, leaving the holes in the valence band. The holes are capable of decomposing the pollutants in the aqueous solution. The photogenerated electrons in CB can reduce the



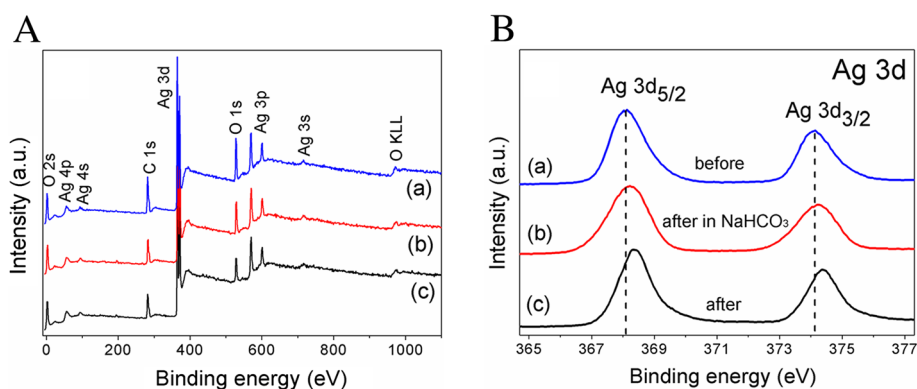


Figure 7 XPS spectra. **(A)** XPS survey spectra and **(B)** high-resolution XPS spectra of Ag 3d of Ag_2CO_3 . Curves (a-c) are XPS results of Ag_2CO_3 before and after photodegradation experiments under visible-light irradiation.

dissolved O_2 in the solution to form H_2O_2 (Equation 1) and also can reduce Ag^+ ions in Ag_2CO_3 to form Ag particles (Equation 2). The formation of large amounts of Ag particles on the surface can result in instability of the Ag_2CO_3 under visible light. Meanwhile, they can also bring the decrease of the photocatalytic activity. In addition, Ag_2CO_3 has a small quantity of dissolution in aqueous solution (Equation 3, Ag^+ : 2.5×10^{-4} M), and the free Ag^+ on the surface may be reduce to Ag^0 (Equation 4). This process may further increase the solubility and promote the instability of Ag_2CO_3 in water.



To avoid the disadvantages of photocorrosion, we employ NaHCO_3 as a stabilizer to inhibit the photocorrosion

and decrease the solubility of Ag_2CO_3 in aqueous solution. So, to further evaluate the photostability of Ag_2CO_3 in the presence of NaHCO_3 , the recycled experiments for the photodegradation of RhB were performed, and the results are shown in Figure 5C. After four cycles, the Ag_2CO_3 still gives 70% degradation rate of RhB after 40-min visible-light irradiation and that the Ag_2CO_3 in the absence of NaHCO_3 almost lost their activity. It indicates that the presence of NaHCO_3 is helpful to enhance the stability and photocatalytic activity of Ag_2CO_3 . On the basis of experimental results, two possible reasons are proposed to explain the significantly enhanced photocatalytic activity and stability of the presence of NaHCO_3 . Firstly, the NaHCO_3 may effectively prevent the dissolution of the Ag_2CO_3 in aqueous solution. More importantly, when the presence of NaHCO_3 , it can facilitate reaction (Equation 2) equilibrium shift to the left and decrease photogenerated electrons reduce Ag^+ ions in Ag_2CO_3 . So, it avoids the formation of large amounts of Ag particles, which lead to the photocatalyst inactivate. However, a small amount of Ag particles on the surface of Ag_2CO_3 can become electron-

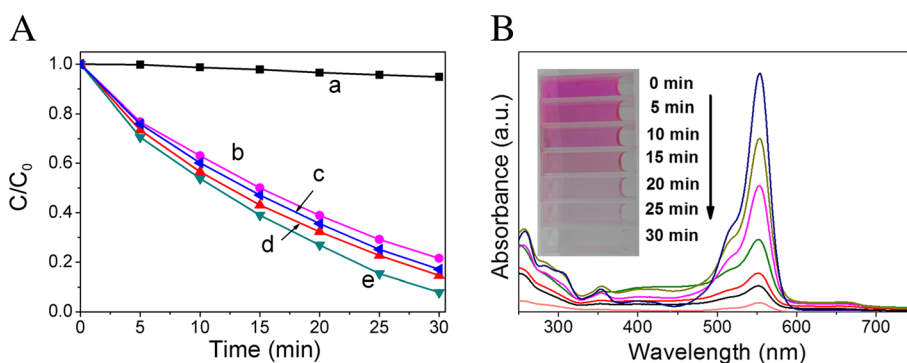


Figure 8 Photocatalytic degradation efficiencies and UV-vis spectral changes. **(A)** The visible-light photocatalytic activity of porous Ag_2CO_3 nanorods in the presence of NaHCO_3 with different concentrations as follows: 0 M (a), 0.1 M (b), 0.001 M (c), 0.01 M (d), and 0.01 M NaHCO_3 in the absence of photocatalysts (a). **(B)** UV-vis absorbance spectral changes of RhB aqueous in as-prepared of porous Ag_2CO_3 nanorods with 0.01 M NaHCO_3 as a function of irradiation time.

rich collective. These electrons will participate in the degradation of pollutants. Thus, it promotes effective separation of electron-hole pairs.

To be more convincing of the possible mechanism, XPS measurements were performed to investigate the changes of chemical state of Ag_2CO_3 before and after photodegradation experiments (Figure 7). The survey XPS spectra are shown in Figure 7A. Carbon, oxygen, and silver were detected in the as-prepared Ag_2CO_3 samples, and no other impurities were found. Furthermore, Figure 7B shows the high-resolution XPS spectrum of Ag 3d region. As-prepared Ag_2CO_3 samples of Ag 3d_{3/2} and Ag 3d_{5/2} photoelectrons at 374.13 and 368.13 eV could be attributed to Ag^+ in Ag_2CO_3 [37,38]. After four cycles of photodegradation experiments in the absence of NaHCO_3 , the Ag 3d_{5/2} peak obvious shifts from 368.13 to 368.33 eV, yet, the Ag 3d_{5/2} peak only shifts to 368.23 eV once the presence of NaHCO_3 . It is stated that a strong covalent bond between Ag^+ cation and the ligand will result lower binding energy of Ag^+ oxidation state than neutral Ag^0 [39,40]. In contrast to the XPS spectra of all Ag 3d_{5/2} (Figure 7B), from curve (a) to (c), the peak shifts to the higher binding energy, which indicates the decrease of the Ag^+ in Ag_2CO_3 oxidation state while the increase of Ag^0 . Meanwhile, the variation tendency confirms the restrained effect of Ag_2CO_3 photocorrosion in the presence of NaHCO_3 from the perspective of experiments.

Furthermore, Figure 8A shows the comparison of visible-light photocatalytic activity of porous Ag_2CO_3 nanorods in the presence of NaHCO_3 with different concentrations. When only in the presence of NaHCO_3 , the RhB solutions almost were not degraded. Further observation shows that the Ag_2CO_3 exhibits the best photocatalytic activity in 0.01 M NaHCO_3 . When the concentration of NaHCO_3 was reduced to 0.001 M, the degradation rate of RhB was decreased. This is due to low concentrations of NaHCO_3 which will not effectively prevent the solubility and photogenerated electrons reduce Ag^+ ions in Ag_2CO_3 . However, in 0.1 M NaHCO_3 , the degradation rate is decrease even further. This may be understood as such, although excess NaHCO_3 effectively prevents photogenerated electrons reduce Ag^+ , at the same time, the photogenerated electrons become difficult to separate from holes. Furthermore, a small amount of Ag particles can be helpful to promote photocatalytic activity. Moreover, the UV-vis absorbance spectral changes of RhB aqueous in porous Ag_2CO_3 nanorods in the presence of 0.01 M NaHCO_3 as a function of irradiation time were investigated (Figure 8B). The maximum absorption wavelengths of RhB solutions are not shifting which indicate that the benzene/heterocyclic rings of the RhB molecule are decomposed [24].

Conclusions

In summary, the novel porous Ag_2CO_3 nanorods were successfully synthesized by using a facile, simple, effective method. The morphology and size of the as-prepared samples can be controlled by adjusting the dispersing agent category and means of adding to reactant. The obtained porous Ag_2CO_3 nanorods exhibit the capability to efficiently catalyze the degradation of organic pollutants under visible-light irradiation. Furthermore, adding an appropriate concentration of NaHCO_3 solution can effectively improve photoactivity and stability of Ag_2CO_3 . Consequently, our work provides a one-pot aqueous solution reaction at room temperature of strategy which may be useful to extend to the synthesis of porous nanorods of other inorganic materials.

Competing interests

The authors declare that they have no competing interests.

Authors' contributions

JB carried out the sample preparation and experimental measurements and drafted the manuscript. SG and LY conceived the work, supervised the experiments, and revised the manuscript. TH and CJ helped to analyze the characterization results. LZ and JP supervised all of the study and provided financial support. All authors read and approved the final manuscript.

Acknowledgements

This work was supported by the Yunnan Provincial Science and Technology Innovation Talents scheme -Technological Leading Talent (NO. 2013HA002) and State International Joint Research Center of Advanced Technology for Superhard Materials (NO.2013B01038).

Author details

¹State Key Laboratory of Complex Nonferrous Metal Resources Clean Utilization, Kunming University of Science and Technology, Kunming 650093, China. ²National Local Joint Laboratory of Engineering Application of Microwave Energy and Equipment Technology, Kunming 650093, China. ³Key Laboratory of Unconventional Metallurgy, Ministry of Education, Kunming 650093, China. ⁴Faculty of Metallurgical and Energy Engineering, Kunming University of Science and Technology, No. 253 Xuefu Rd., Kunming 650093, China.

Received: 29 January 2015 Accepted: 7 April 2015

Published online: 21 April 2015

References

1. Zhang H, Chen G, Bahnemann DW. Photoelectrocatalytic materials for environmental applications. *J Mater Chem*. 2009;19:5089–121.
2. Teoh WY, Scott JA, Amal R. Progress in heterogeneous photocatalysis: from classical radical chemistry to engineering nanomaterials and solar reactors. *J Phys Chem Lett*. 2012;3:629–39.
3. Kamat PV, Bisquert J. Solar fuels. Photocatalytic hydrogen generation. *J Phys Chem C*. 2013;117:14873–5.
4. Fujishima A, Rao TN, Tryk DA. Titanium dioxide photocatalysis. *J Photochem Photobiol C*. 2000;1:1–21.
5. Chen X, Mao SS. Titanium dioxide nanomaterials: synthesis, properties, modifications, and applications. *Chem Rev*. 2007;107:2891–959.
6. Paramasivam I, Jha H, Liu N, Schmuki P. A review of photocatalysis using self-organized TiO_2 nanotubes and other ordered oxide nanostructures. *Small*. 2012;8:3073–103.
7. Fresno F, Portela R, Suárez S, Coronado JM. Photocatalytic materials: recent achievements and near future trends. *J Mater Chem A*. 2014;2:2863–84.
8. Li Y, Zhang L, Wu W, Dai P, Yu X, Wu M, et al. Hydrothermal growth of TiO_2 nanowire membranes sensitized with CdS quantum dots for the enhancement of photocatalytic performance. *Nanoscale Res Lett*. 2014;9:1–6.

9. Scuderi V, Impellizzeri G, Romano L, Scuderi M, Nicotra G, Bergum K, et al. TiO₂-coated nanostructures for dye photo-degradation in water. *Nanoscale Res Lett*. 2014;9:1–7.
10. Akpan UG, Hameed BH. Development and photocatalytic activities of TiO₂ doped with Ca-Ce-W in the degradation of acid red 1 under visible light irradiation. *Desalin Water Treat*. 2013;52:5639–51.
11. Ouyang S, Kikugawa N, Chen D, Zou Z, Ye J. A systematic study on photocatalytic properties of AgMO₃ (M = Al, Ga, In): effects of chemical compositions, crystal structures, and electronic structures. *J Phys Chem C*. 2009;113:1560–6.
12. Singh J, Uma S. Efficient photocatalytic degradation of organic compounds by ilmenite AgSbO₃ under visible and UV light irradiation. *J Phys Chem C*. 2009;113:12483–8.
13. Li G, Yan S, Wang Z, Wang X, Li Z, Ye J, et al. Synthesis and visible light photocatalytic property of polyhedron-shaped AgNbO₃. *Dalton T*. 2009;8519–24.
14. Wu W, Liang S, Chen Y, Shen L, Yuan R, Wu L. Mechanism and improvement of the visible light photocatalysis of organic pollutants over microcrystalline AgNbO₃ prepared by sol–gel method. *Mater Res Bull*. 2013;48:1618–26.
15. Liu W, Liu X, Fu Y, You Q, Huang R, Liu P, et al. Nanocrystalline pyrochlore AgSbO₃: hydrothermal synthesis, photocatalytic activity and self-stable mechanism study. *Appl Catal B Environ*. 2012;123:78–83.
16. Liu Y, Yu H, Cai M, Sun J. Microwave hydrothermal synthesis of Ag₂CrO₄ photocatalyst for fast degradation of PCP-Na under visible light irradiation. *Catal Commun*. 2012;26:63–7.
17. Xu D, Cao S, Zhang J, Cheng B, Yu J. Effects of the preparation method on the structure and the visible-light photocatalytic activity of Ag₂CrO₄. *Beilstein J Nanotech*. 2014;5:658–66.
18. Dong C, Wu KL, Wei XW, Wang J, Liu L, Hu Y, et al. Preparation of Ag₂SO₃ sub-microparticles with high visible-light photocatalytic activity. *Micro Nano Lett*. 2014;9:417–20.
19. Tang J, Liu Y, Li H, Tan Z, Li D. A novel Ag₃AsO₄ visible-light-responsive photocatalyst: facile synthesis and exceptional photocatalytic performance. *Chem Commun*. 2013;49:5498–500.
20. Dong H, Li Z, Xu X, Ding Z, Wu L, Wang X, et al. Visible light-induced photocatalytic activity of delafossite AgMO₂ (M = Al, Ga, In) prepared via a hydrothermal method. *Appl Catal B Environ*. 2009;89:551–6.
21. Tang J, Li D, Feng Z, Tan Z, Ou B. A novel AgIO₄ semiconductor with ultrahigh activity in photodegradation of organic dyes: insights into the photosensitization mechanism. *RSC Adv*. 2014;4:2151–4.
22. Xu C, Liu Y, Huang B, Li H, Qin X, Zhang X, et al. Preparation, characterization, and photocatalytic properties of silver carbonate. *Appl Surf Sci*. 2011;257:8732–6.
23. Dai G, Yu J, Liu G. A new approach for photocorrosion inhibition of Ag₂CO₃ photocatalyst with highly visible-light-responsive reactivity. *J Phys Chem C*. 2012;116:15519–24.
24. Dong H, Chen G, Sun J, Li C, Yu Y, Chen D. A novel high-efficiency visible-light sensitive Ag₂CO₃ photocatalyst with universal photodegradation performances: Simple synthesis, reaction mechanism and first-principles study. *Appl Catal B Environ*. 2013;134:46–54.
25. Pan JH, Dou H, Xiong Z, Xu C, Ma J, Zhao XS. Porous photocatalysts for advanced water purifications. *J Mater Chem*. 2010;20:4512–28.
26. Li Y, Fu ZY, Su BL. Hierarchically structured porous materials for energy conversion and storage. *Adv Funct Mater*. 2012;22:4634–67.
27. Wang JL, Wang C, Lin W. Metal-organic frameworks for light harvesting and photocatalysis. *ACS Catal*. 2012;2:2630–40.
28. Chi B, Zhao L, Jin T. One-step template-free route for synthesis of mesoporous N-doped titania spheres. *J Phys Chem C*. 2007;111:6189–93.
29. Dollimore D, Spooner P, Turner A. The BET method of analysis of gas adsorption data and its relevance to the calculation of surface areas. *Surf Tech*. 1976;4:121–60.
30. Boissière C, van der Lee A, El Mansouri A, Larbot, A, Prouzet, E. A double step synthesis of mesoporous micrometric spherical MSU-X silica particles. *Chem Commun*. 1999. 2047–8.
31. Martines MU, Yeong E, Persin M, Larbot A, Voorhout WF, Kübel C, et al. Hexagonal mesoporous silica nanoparticles with large pores and a hierarchical porosity tested for HPLC. *Comptes Rendus Chimie*. 2005;8:627–34.
32. Chen D, Liu M, Chen Q, Ge L, Fan B, Wang H, et al. Large-scale synthesis and enhanced visible-light-driven photocatalytic performance of hierarchical Ag/AgCl nanocrystals derived from freeze-dried PVP–Ag⁺ hybrid precursors with porosity. *Appl Catal B Environ*. 2014;144:394–407.
33. Cao M, Li C, Zhang B, Huang J, Wang L, Shen Y. PVP assisted solvothermal synthesis of uniform Cu₂FeSnS₄ nanospheres. *J Alloy Compd*. 2015;622:695–702.
34. Zeng X, Zhou B, Gao Y, Wang C, Li S, Yeung CY, et al. Structural dependence of silver nanowires on polyvinyl pyrrolidone (PVP) chain length. *Nanotechnology*. 2014;25:495601.
35. Wang Y, Huang D, Zhu X, Ma Y, Geng H, Wang Y, et al. Surfactant-free synthesis of Cu₂O hollow spheres and their wavelength-dependent visible photocatalytic activities using LED lamps as cold light sources. *Nanoscale Res Lett*. 2014;9:1–8.
36. Yu C, Li G, Kumar S, Yang K, Jin R. Phase transformation synthesis of novel Ag₂O/Ag₂CO₃ heterostructures with high visible light efficiency in photocatalytic degradation of pollutants. *Adv Mater*. 2014;26:892–8.
37. Xu H, Zhu J, Song Y, Zhao W, Xu Y, Song Y, et al. Ion-exchange preparation for visible-light-driven photocatalyst AgBr/Ag₂CO₃ and its photocatalytic activity. *RSC Adv*. 2014;4:9139–47.
38. Xu H, Zhu J, Song Y, Zhu T, Zhao W, Song Y, et al. Fabrication of AgX-loaded Ag₂CO₃ (X = Cl, I) composites and their efficient visible-light-driven photocatalytic activity. *J Alloy Compd*. 2015;622:347–57.
39. MeeLee J, KyungJo Y. A facile exfoliation-crystal growth route to multicomponent Ag₂CO₃/Ag-Ti₃NbO₁₄ nanohybrids with improved visible light photocatalytic activity. *Dalton T*. 2014;43:10566–73.
40. Gaarenstroom SW, Winograd N. Initial and final state effects in the ESCA spectra of cadmium and silver oxides. *J Chem Phys*. 1977;67:3500–6.

Submit your manuscript to a SpringerOpen[®] journal and benefit from:

- Convenient online submission
- Rigorous peer review
- Immediate publication on acceptance
- Open access: articles freely available online
- High visibility within the field
- Retaining the copyright to your article

Submit your next manuscript at ► springeropen.com
